

Nonlinear Optics in Porous Silicon Photonic Crystals and Microcavities

M. G. Martemyanov¹, D. G. Gusev¹, I. V. Soboleva¹, T. V. Dolgova¹, A. A. Fedyanin¹,
O. A. Aktsipetrov¹, and G. Marowsky²

¹ Department of Physics, Moscow State University, Moscow, 119992 Russia

e-mail: fedyanin@shg.ru

² Laser-Laboratorium Göttingen, Göttingen, 37077 Germany

Received October 22, 2003

Abstract—This paper is a survey of our recently published and new results on nonlinear-optical studies of photonic band-gap (PBG) structures formed from mesoporous silicon. The studies are performed on photonic crystals, high-quality-factor microcavities (MC) with a half-wavelength-thick microcavity spacer, and on series of coupled microcavities with two identical microcavity spacers and controllable coupling by intermediate Bragg reflector transmittance. The enhanced second-harmonic generation (SHG) is observed and analyzed for the fundamental wavelength at the PBG edge and in resonance with the microcavity mode. The second-harmonic intensity is enhanced by a factor of approximately 10^2 in comparison with that outside the photonic band gap. The interrelation of two enhancement mechanisms, spatial field localization and phase matching, is determined. The dependence of the shape of SHG spectra on coupling is studied at resonance with one of the splitted modes of coupled microcavities. The experimental results on third-harmonic generation in PBG materials are presented. The resonant enhancement is observed both at the PBG edge and in the MC mode. The intensity achieves 10^3 at the photonic band-gap edge and 5×10^3 in the MC mode in comparison with an off-resonant value. A peculiar factor is the interplay of silicon absorption and the cubic susceptibility resonance at the third-harmonic wavelength near the E'_0/E_1 critical point of silicon.

1. INTRODUCTION

In nonlinear processes, an important role is played by the phase relations between interacting waves. The presence of dispersion leads to limitation of the effective interaction length to the value of the coherence length. For example, this is the key factor for parametric processes of harmonics generation. There are several well-known methods for compensating for phase mismatch. One of them is based on birefringency utilizing different group velocities of ordinary and extraordinary waves [1]. Another technique is spatial modulation of $\chi^{(2)}$ with a period of the coherence length, for example, $\chi^{(2)}$ sign inversion by spatially periodical external field poling of a ferroelectric material [2]. The second factor influencing the nonlinear response is optical-field enhancement via spatial or time localization. For example, surface-enhanced Raman scattering, giant second-harmonic generation (SHG), and giant Raman scattering by metal nanoparticles and cold noble metal films are illustrations of local-field enhancement [3]. Photonic band-gap (PBG) structures allow manipulation of both phase relations and local field [4]. Compression of femtosecond pulses in one-dimensional photonic crystals (PCs) [5], field enhancement for a particular wavelength at the PBG edge [6] or localization at a defect cell have been demonstrated. Effective four-wave mixing is observed in a PC at the PBG edge. Raman scattering enhancement by one-dimensional photonic-crystal microcavities (MCs) was

studied in [7, 8]. Effective compensation of phase mismatch in multilayers was proposed as far back as in 1962 by Bloembergen [9] and observed later in Bragg reflectors formed from different materials [10–14]. Third-harmonic generation in a PC is described theoretically both by the direct coupling via the cubic susceptibility [15] and by cascade processes of second-harmonic and sum-frequency generation [16]. One of the convenient materials for fabrication one-dimensional PBG structures is porous silicon (PS), which allows easily controllable variations of the optical thickness and refractive index of a particular layer [17]. Proper layer periodicity and sharp internal interfaces can be achieved, resulting in bright effects, such as narrow strong photoluminescence [18], manifold enhanced Raman scattering [7], and harmonics generation [19, 20]. PS samples with a complicate structure of double or multiple spacers can be fabricated with a high quality factor of resonances [21, 22].

In this paper, the enhanced quadratic and cubic nonlinear-optical response is studied in three classes of one-dimensional PBG structures: photonic crystals, photonic-crystal microcavities [14], and coupled microcavities (CMC) formed from mesoporous silicon with controllable coupling [23]. The enhancement mechanisms of quadratic (second-harmonic generation) [19] and degenerated four-wave mixing (third-harmonic generation (THG)) [24] are analyzed.

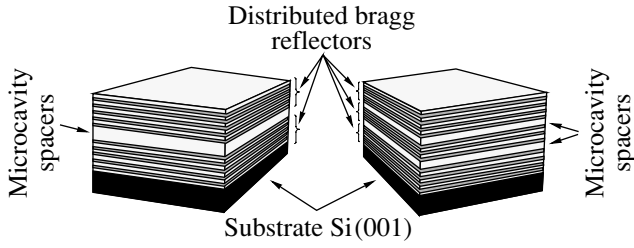


Fig. 1. (Left) Sketch of the MC sample; (right) sketch of the CMC sample.

The paper is organized as follows. Section 2 contains the phenomenological description of SHG and THG mechanisms in PS. In Section 3, the details of fabrication of single and coupled PS microcavities and the experimental setups employed are presented. In Section 4, the experimental results of the SHG and THG spectroscopy of single and coupled microcavities in frequency and wave-vector domains are shown and discussed. Section 4 also contains numerical results in MCs and CMC and a comparison of the SHG experiment and model. All results are summarized in Section 5.

2. BACKGROUND

The type of nonlinear sources in PS (electric dipole or quadrupole) and the localization (the PS surface or bulk) have been intensively discussed in the literature [25, 26]. The dipole contribution to quadratic polarization can be induced at the PS interfaces as well as at inner pores surfaces, where inversion symmetry of bulk silicon is necessarily broken. The quadrupole term is expected from the bulk of silicon nanocrystals forming PS, and the nonlocal quadrupole-type contribution can stem from the inner pore surface due to large field gradients at silicon–air interfaces. The experiments show that the mechanism of dipole nonlinear sources uniformly distributed over the bulk of each PS layer can be taken [19]. The corresponding symmetry group of the individual PS layer is supposed to be ∞m . The effective dipole quadratic polarization inside the j th PS layer is given by

$$\mathbf{P}_j^{2\omega}(z) = \hat{\chi}^{(2),j} : \mathbf{E}_j^\omega(z) \mathbf{E}_j^\omega(z), \quad (1)$$

with three nonzero independent components of the second-order susceptibility tensor of the j th layer, $\hat{\chi}^{(2),j}$:

$$\begin{aligned} \chi_1 &\equiv \chi_{xzx} = \chi_{zyz} = \chi_{xxz} = \chi_{yyz}, \\ \chi_2 &\equiv \chi_{zxx} = \chi_{zyy}, \\ \chi_3 &\equiv \chi_{zzz}. \end{aligned} \quad (2)$$

These components determine the presence of the SHG signal only for the s -in, s -out and p -in, p -out polarization combinations.

The THG can be observed only for the p -in, p -out and s -in, s -out polarization combinations. The TH

intensity in the p -in, s -out and s -in, p -out polarization combinations is negligible. The electric-dipole cubic polarization, $\mathbf{P}^{(3)}(3\omega) = \chi^{(3)} : \mathbf{E}(\omega) \mathbf{E}(\omega) \mathbf{E}(\omega)$, is supposed to be the only source of THG in porous silicon MCs. Cascade THG is neglected since small electric-dipole SHG is expected only at the pore surfaces due to the inversion symmetry of the bulk silicon. Each porous silicon layer is considered as macroscopically in-plane isotropic having nine nonzero $\chi^{(3)}$ elements:

$$\begin{aligned} \chi_{yyzz}^{(3)} &= \chi_{xxzz}^{(3)}, \quad \chi_{zzzz}^{(3)}, \\ \chi_{zzxx}^{(3)} &= \chi_{zzyy}^{(3)}, \\ \chi_{ijij}^{(3)} &= 1/3 \chi_{iiii}^{(3)}, \end{aligned} \quad (3)$$

with $i, j = x, y$.

3. SAMPLES

Photonic crystals and microcavities are fabricated by the conventional electrochemical etching procedure [17] using p^+ -type doped (0.005 Ω cm) Si(001) wafers in electrolyte containing 15% fluoric acid, 27% water, and 58% ethanol. After chemical removal of the native oxide, the silicon wafer is set into the electrochemical cell and tightly clamped by its backside to a flat copper cathode. The platinum spiral anode is immersed into the electrolyte. The modulation of the refractive index along the surface normal z is achieved by time variation of the etching current. The thickness of the mesoporous silicon layers is controlled by the etching time. The optical thickness of the layers is obtained using the refractive index values calculated within the effective medium approximation [27]. Atomic force microscope images show that the pore size is significantly smaller than the optical wavelength.

The MC samples consist of a half-wavelength-thick microcavity spacer ($\lambda_{MC} \approx 1300, 1200, \text{ and } 940$ nm) sandwiched between two distributed Bragg reflectors formed from five pairs of quarter-wavelength-thick layers (Fig. 1). λ_{MC} denotes spectral position of microcavity mode, that is the double optical thickness of the microcavity spacer. The refractive indices of the layers in the Bragg reflectors are $n_H \approx 1.79$ and $n_L \approx 1.42$, and the porosities are $f_H \approx 0.64$ and $f_L \approx 0.77$, respectively. The refractive index of the microcavity spacer is $n_{MC} = n_L$. The Q factor is slightly below 10^2 and is restricted by losses due to light scattering in the pores.

The CMC samples consist of three photonic crystals, separated by two identical $\lambda_{MC}/2$ -thick spacers $\lambda_{MC} \approx 1200$ nm (Fig. 1). External Bragg reflectors are formed from four pairs of $\lambda_{MC}/4$ -thick layers of porous silicon. The number of layers in the intermediate Bragg reflector (IBR), N , is changed in series from three to nine. The refractive index of spacers is n_L . The CMC with $N = 5$ and the same refraction indices, but with λ_{MC}

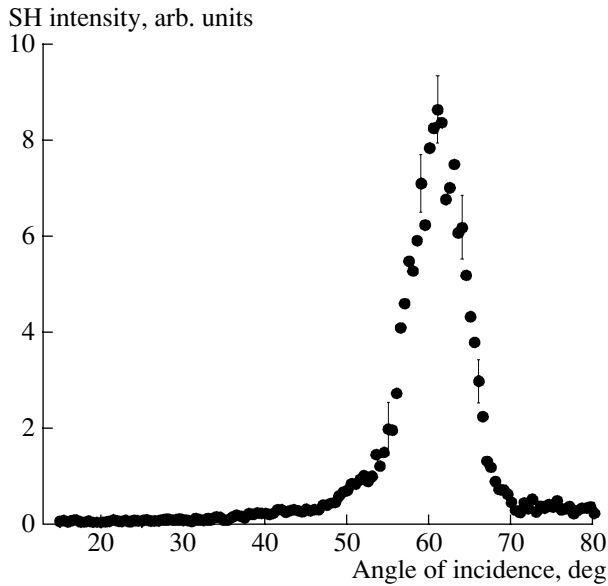


Fig. 2. The SHG angular spectrum of the photonic crystal with PBG centered at 1200 nm.

shifted to 800 nm, is fabricated for linear reflection spectroscopy in the wavelength domain.

Tuning the fundamental radiation across the PBG edge and resonance of the fundamental wave with the MC mode, $k_z d_{MC} = \pi$, where k_z is the normal component of the fundamental wave vector inside the MC spacer, are achieved in both frequency and wave-vector domains. SHG and THG spectroscopy in the frequency domain is realized by tuning the fundamental wavelength λ_ω at a fixed angle of incidence θ . In the wave-vector domain SHG and THG spectroscopy, θ is varied at fixed λ_ω . The 4-ns-pulsed output of the optical parametric oscillator tunable from 750 to 1300 nm and the 10-ns-pulsed infrared output of the Nd³⁺:YAG laser are used, respectively. The energy of fundamental radiation is below 5 mJ/pulse. The radiation reflected from the sample passes through color and interference filters, which extract the SH or TH light, and a Glan prism separating the required polarization. A monochromator is used to check the spectral background. Since there is high UV absorption of the silicon substrate, only the reflected TH and SH radiation is detected.

4. RESULTS AND DISCUSSION

4.1. SHG in Photonic Crystals and Microcavities

4.1.1. Photonic crystals and microcavities. Figure 2 shows the angular spectrum of intensity of the SH generated by the photonic crystal with PBG centered at 1200 nm for normal incidence. This spectrum reveals a peak at 60° related to the right edge of the PBG. The peak of the SH intensity results from the homogeneous enhancement of the fundamental field and achievement of the phase-matching condition [13, 28]. Figure 3a

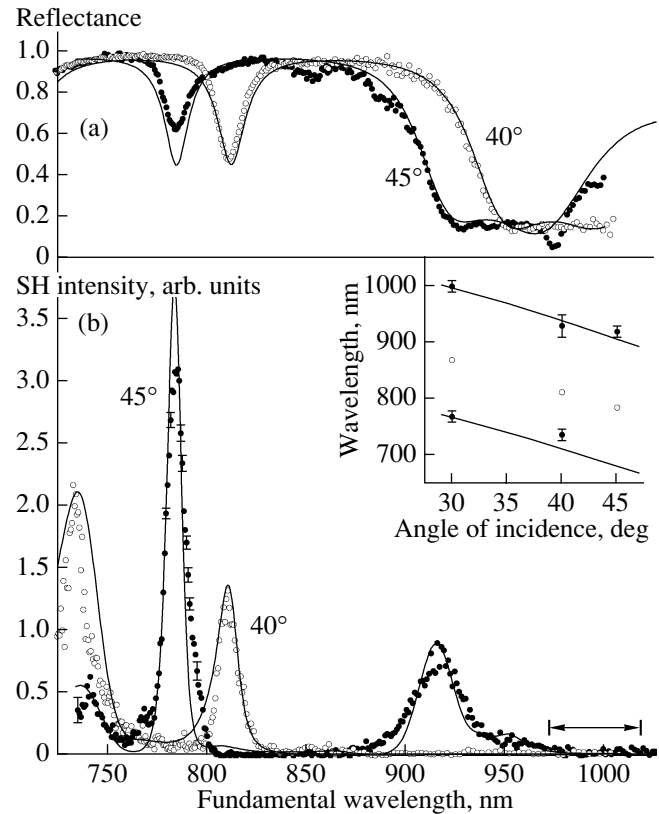


Fig. 3. (a) The linear reflection spectra of the PS microcavity measured for various angles of incidence. (b) The SHG spectra for $\theta = 45^\circ$ (solid circles) and $\theta = 40^\circ$ (empty circles). The curves are the result of the combined fit to linear reflection and SHG spectra. Inset: Angular dependence of positions of SHG peaks at the MC mode (open circles) and the PBG edges (filled circles), and the calculated angular dependences of the PBG edges (lines).

shows the linear spectra of the *s*-polarized fundamental radiation reflected from MC with $\lambda_{MC} = 945$ nm. The spectra have a plateau with almost full reflection corresponding to PBG and a dip related to the MC mode. Figure 3b shows the SH intensity spectra acquired for this MC in *s*-in, *p*-out geometry. The SH intensity is strongly enhanced at $\lambda_\omega \approx 785$ nm for $\theta = 45^\circ$ and at $\lambda_\omega \approx 810$ nm for $\theta = 40^\circ$, as the fundamental field is in resonance with the mode, i.e., if $\lambda_\omega =$

$\lambda_{MC} \sqrt{1 - n_{MC}^{-2} \sin^2 \theta}$, where n_{MC} is the refractive index of the MC spacer. The largest enhancement is detected for $\theta = 45^\circ$ and is 130 times on comparison with that averaged outside PBG in the λ_ω interval from 975 to 1025 nm and indicated in Fig. 3b by the arrow. Two other spectral features at $\lambda_\omega \approx 915$ nm for $\theta = 45^\circ$ and at $\lambda_\omega \approx 735$ nm for $\theta = 40^\circ$ correspond to both PBG edges. As θ decreases to 30° , SHG peaks redshift (inset to Fig. 3b) in accordance with the angular dependence of the spectral positions of the PBG edges and the MC mode. The large difference in the magnitude of the SHG peaks at the PBG edges for $\theta = 40^\circ$ is most likely

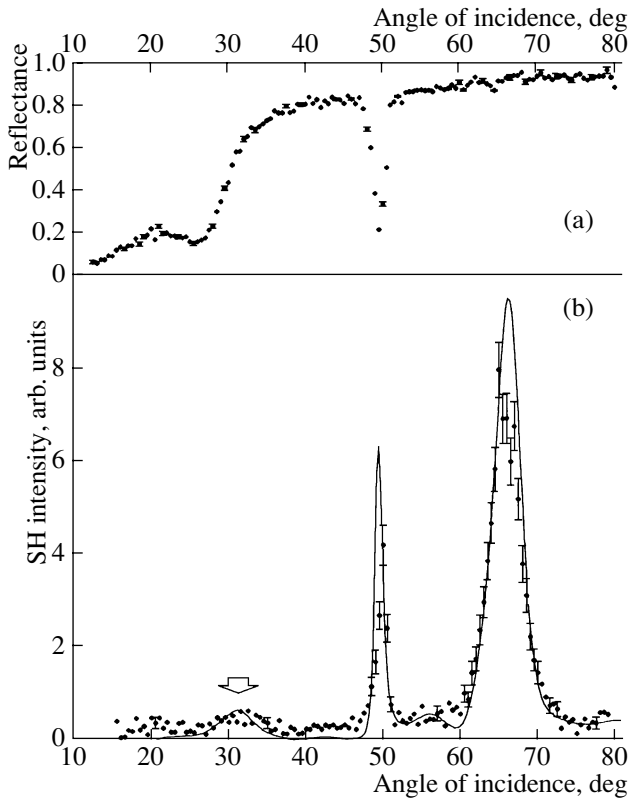


Fig. 4. (a) Angular spectrum of the *s*-polarized fundamental wave reflected from MC with $\lambda_{MC} = 1350$ nm. (b) SHG angular spectrum of this MC. The arrow emphasizes the SHG peak at the low-angle PBG edge. The curve is the result of model calculations.

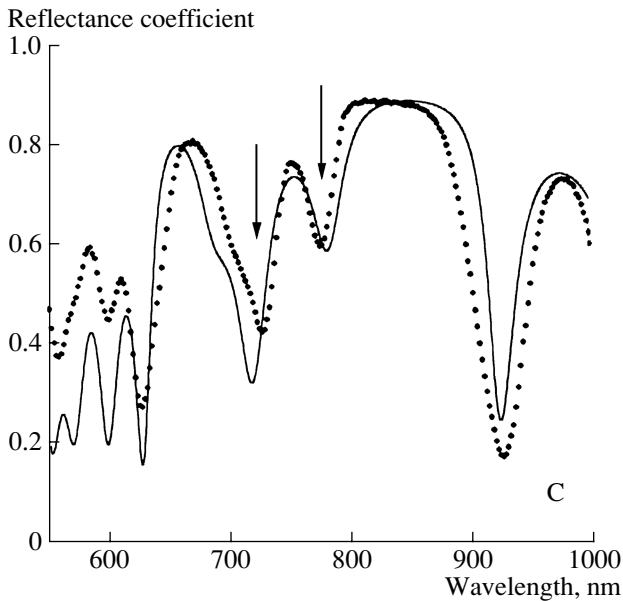


Fig. 5. Reflection spectrum of the porous silicon CMC with $\lambda_{MC} \approx 800$ nm and $N = 5$ measured for a 45° angle of incidence of the *s*-polarized wave. The curve is the fit to the data by the transfer-matrix formalism. Arrows indicate the eigenmode positions.

associated with the two-photon resonance of PS quadratic susceptibility related to the E'_0/E_1 critical point of the crystalline silicon band structure.

The MC confinement of the fundamental field is also achieved by tuning the angle of incidence of the fundamental radiation with fixed wavelength. Figures 4a and 4b show the angular spectra of the linear reflection coefficient at $\lambda_\omega = 1064$ nm and the SH intensity acquired for MC with $\lambda_{MC} = 1350$ nm. The SHG angular spectrum has a narrow peak at $\theta \approx 50^\circ$ corresponding to a dip in the linear reflection spectrum and attributed to the fundamental field resonance with the MC mode. The two broader SHG peaks at 30° and 65° are related to the PBG edges. The edge at large θ values is unresolved in Fig. 4a due to the strong angular dependence of the Fresnel factors. However, the SHG angular spectrum presented in Fig. 2 reveals a peak with a similar angular width and position to those of the SHG peak at 65° for MC. The different magnitude of the SHG peaks at the PBG edges is a result, in part, of the angular dependence of the isotropic SHG component [29]. The calibration of the resonant SHG signal from MC is performed using the Si(001) substrate. The SH intensity in the maximum of the SHG angular spectrum measured at this silicon surface in a *p*-in, *p*-out polarization combination is at least 150 times smaller.

4.1.2. Coupled microcavities. The linear reflection spectrum of the porous silicon CMC measured in the wavelength domain is shown in Fig. 5. The spectrum has a plateau with high reflectivity, corresponding to the PBG, and two resonant dips at approximately 730 and 780 nm. These drops in the reflection coefficient correspond to the split CMC modes, since the fundamental radiation resonant with the CMC eigenmodes propagates efficiently in CMC and is localized into and in the vicinity of spacers, as is shown in Figs. 6a and 6b.

Figure 7 shows the angular spectra of the fundamental wave reflection and the SH intensity measured for the series of porous silicon CMC with different reflectivity of the intermediate Bragg reflector. The linear spectra have two dips, where the reflection coefficient value decreases up to 0.2, corresponding to the resonance of the fundamental radiation with the CMC modes. In the other parts of the spectra, the reflection coefficient reaches the values of up to 0.85, which corresponds to the PBG. For all CMC samples, the right dip in the spectra related to the long-wavelength mode of CMC is shallower than the left one, that can be attributed to the monotonous decrease in the optical thickness of porous silicon layers with the depth [30].

The angular spectra of the SH intensity have resonant features in the range of θ from 20° to 70° . $\theta_S^{\omega(2\omega)}$ and $\theta_L^{\omega(2\omega)}$ denote angular positions of resonance features in linear and SHG spectra corresponding to the short- and long-wavelength modes of CMC, respec-

tively. The angular positions of the SHG peaks at $\theta_S^{2\omega}$ and $\theta_L^{2\omega}$ correlate with the CMC mode positions defined from the reflection spectra of fundamental radiation. However, they are slightly shifted from the positions of the dips in the linear reflection coefficient and are located mostly on their external slopes. The SH intensity increases up to two orders of magnitude in comparison with the SHG signal in the PBG. For all CMC samples, the amplitude of the SHG peak at $\theta_L^{2\omega}$ exceeds the SHG enhancement in the peak at $\theta_S^{2\omega}$. The full width at half maximum (FWHM) of the long-wavelength peaks increases with the decrease in R from approximately 9° for CMC with $N = 9$ to 16° for the sample with $N = 3$. An additional buildup of SH intensity at approximately 65° is observed in the SHG spectra of the CMC samples with $N = 7$ and $N = 9$. The angular splitting of dips in the reflection spectra and SHG peaks as a function of the thickness of the intermediate Bragg reflector is shown in Fig. 8. It decreases gradually with the increase in the IBR reflectivity, that characterizes the reduction of the coupling between microcavities.

The observed SHG enhancement is caused by the increase in the amplitude of the resonant fundamental field inside CMC. The spatial distributions of the field strength along the periodicity direction z are shown in Figs. 6a and 6b. They are calculated for CMC with $N = 5$ by using the transfer-matrix formalism with the plane $z = 0$ corresponding to the CMC–air interface. The fundamental field amplitude in the spacer centers is approximately tenfold enhanced in comparison with that of the incident wave. Since fundamental field localization inside the microcavity spacers is maximal at the resonance with the CMC modes, the angular positions of the SHG peaks are located nearby the dips of the linear reflection spectra. The fundamental field is enhanced both in spacers and in surrounding layers of the Bragg reflectors, and the nonlinear sources contributing to SHG are extended over a micron-size distance. Thus, the magnitude and shape of the SHG peaks are influenced significantly by the interference of the partial contributions to the total outgoing SH field from various layers of CMC. The phases of these partial SH fields, calculated within the nonlinear transfer-matrix formalism [31], depend essentially on the spectral position of CMC modes governed by the refractive indices and thicknesses of porous silicon layers. It is shown that destructive interference of the SHG partial contributions results in the splitting of the SHG peaks at the long-wavelength mode for the sample with $N = 7$ and $N = 9$ and in the changes in their amplitudes. Interference effects also define the spectral shift of the SHG resonances from the dip minima of the linear reflection spectra.

SHG spectra are fitted within the nonlinear transfer-matrix formalism. The effective dipole quadratic sus-

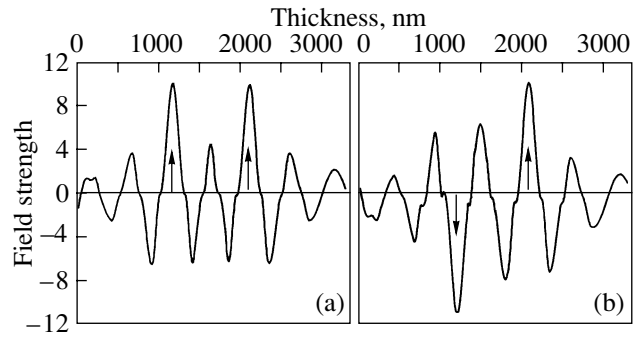


Fig. 6. (a, b) Spatial distribution across porous silicon CMC of the field strength of the optical wave resonant with short-wavelength (panel a) and long-wavelength (panel b) CMC modes. The incident wave amplitude is equal to unity. Dashed lines indicate the interfaces between porous silicon layers. Arrows emphasize the field phases in the spacer centers.

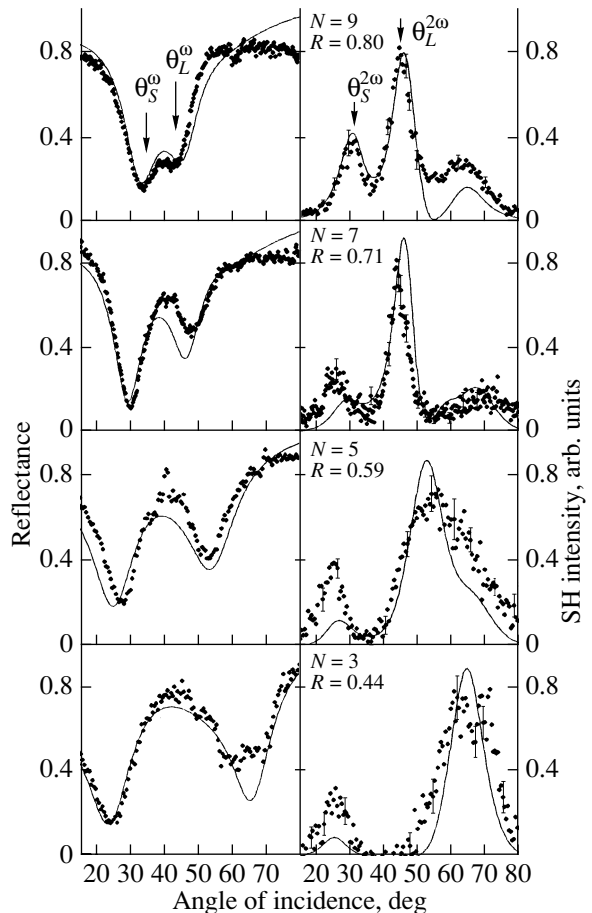


Fig. 7. Angular spectra of SH intensity (right panels) and linear reflection coefficient (left panels) of porous silicon CMC with $\lambda_{MC} \approx 1200$ nm and a different reflection coefficient of IBR, R . Lines are the results of fitting by the transfer-matrix formalism.

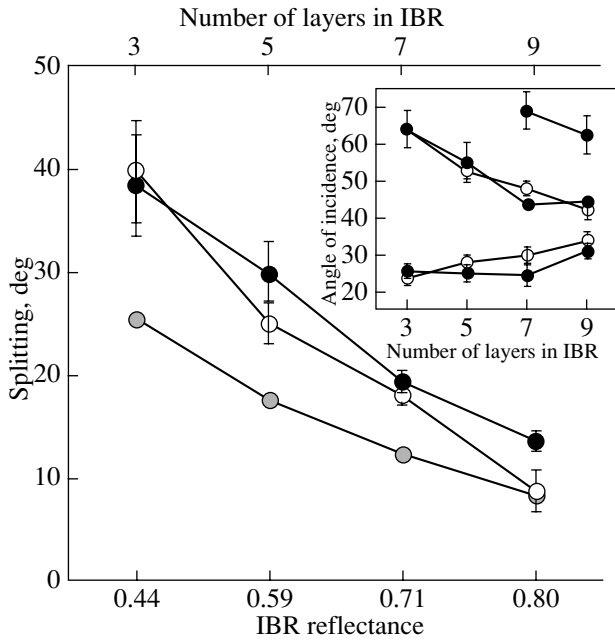


Fig. 8. Dependences of the angular splitting of the SHG resonances, $\theta_L^{2\omega} - \theta_S^{2\omega}$ (filled circles), and the linear reflection coefficient dips, $\theta_L^\omega - \theta_S^\omega$ (empty circles), on the number of layers in the intermediate Bragg reflector and its reflection coefficient. Shaded circles show the model dependence of the splitting of the linear reflection coefficient dips for an ideal CMC. Inset: Angular positions of SHG and linear reflection resonances.

ceptibility of mesoporous silicon layers in CMC, $\chi^{(2),j}$, that arise due to the inversion symmetry breaking at the pore walls is supposed to be constant inside each j th layer [14] and depends on porosity proportionally to $1 - f_j$. The $\chi^{(2)}$ contributions from opposite pore walls no longer interfere destructively, as it was in microporous silicon, since the pore size in mesoporous silicon is of the order of several tens of nanometers.

Macroscopically, this leads to the $\chi_{zxx}^{(2),j} = \chi_{zyy}^{(2),j}$ non-zero elements of $\chi^{(2),j}$ for the s -in, p -out polarization combination related to the medium that is isotropic in the xy plane. The model spectra of the reflection coefficient and the SH intensity are calculated for the ideal CMC structure, in which the optical thicknesses of the layers of Bragg reflectors are equal to $\lambda_{MC}/4$ exactly and the layer thicknesses are taken to be $D_H^{\lambda/4} = 212$ nm and $D_L^{\lambda/4} = 169$ nm for $\lambda_{MC} = 1200$ nm. The curves fit well the SHG resonances and drops in the linear spectra but demonstrate higher quality factors for resonances and smaller splitting values, as shown in Fig. 8. This indicates that the Bragg reflectors in the real CMC have a smaller reflectivity than expected. Better agreement with the data is achieved if corrections are taken accounting for the increase in porosity and decrease in

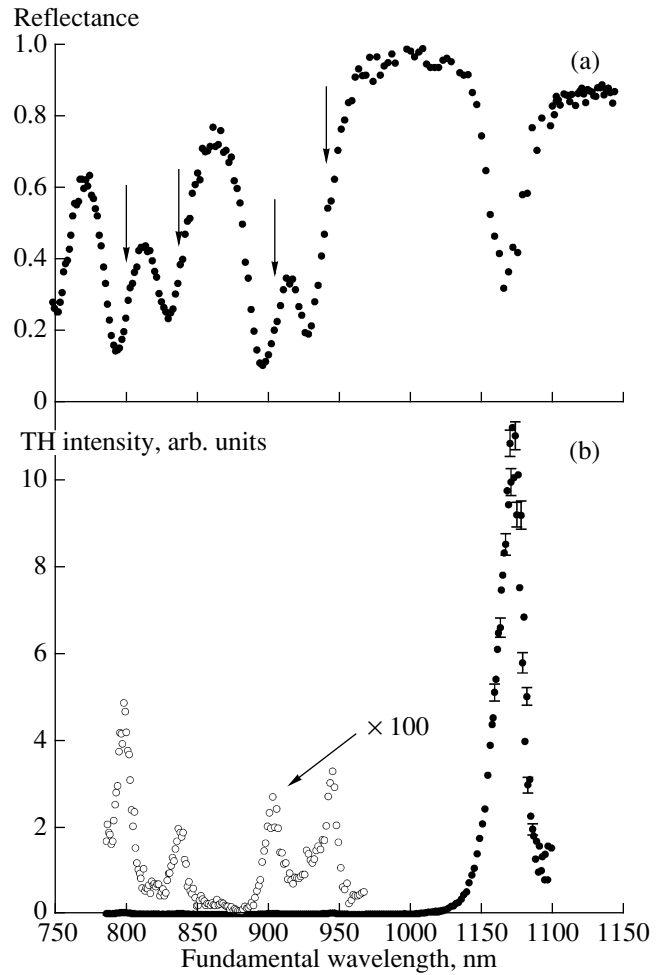


Fig. 9. (a) Linear spectrum of the s -polarized fundamental radiation reflected from porous silicon microcavity. Arrows indicate positions of the peaks in the THG spectrum. (b) (filled circles) THG spectrum of MC measured in the s -in, s -out polarization combination; (empty circles) Part of the spectrum magnified 100 \times .

the refraction index of porous silicon layers with depth [22]. The porosity modulation is caused by the inhomogeneity of the etching process with the depth and the gradual porous silicon oxidation [30] inside the CMC samples. The curves in Fig. 7 show the results of simultaneous fit of the spectra achieved with the same parameters for all CMC samples. The best agreement with the data is obtained with parabolic modulation of the porosity. The porosity of the j th layer is taken as $f_j = f_{0,j} + A \left(1 - \left(\frac{K-j}{K} \right)^2 \right)$, where $f_{0,j}$ is the initial porosity, K is the total number of layers, and A is the maximal porosity modulation. The maximal deviation of the refractive index of the deepest layer from the ideal model does not exceed 0.05. A similar result is achieved by reducing the layer thickness with depth: the deeper layers have smaller thickness than the layers near the

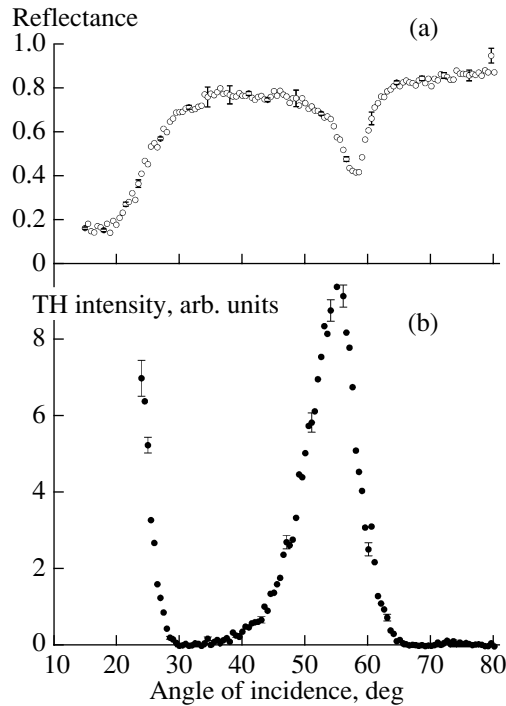


Fig. 10. Angular THG spectrum of the porous silicon MC measured in the *p*-in, *p*-out polarization combination (filled circles); linear reflection spectrum of *s*-polarized fundamental radiation of 1064 nm (open circles).

surface of the sample. The fit of the experimental spectra with a small parabolic deviation of the parameters of the CMC samples with depth can be used for updating the technique of preparation of photonic crystals and microcavities based in porous silicon.

4.2. THG in Photonic Crystals and Microcavities

Figure 9 shows reflection and THG spectra measured in the frequency domain at $\theta = 45^\circ$. The PBG is located at $\lambda_\omega > 950$ nm, where reflectance is close to unity, and the MC mode is centered at $\lambda_\omega \approx 1072$ nm. The THG spectrum has a strong peak which coincides with the MC mode. The TH intensity is approximately 5×10^3 times larger in comparison with that in the pass band. The other THG peaks, magnified in Fig. 9b, are approximately 500 times smaller. They correlate with the minima in the linear reflection spectrum being slightly redshifted. The largest shift of approximately 15 nm is observed at the short-wavelength PBG edge. THG is strongly suppressed out of these peaks in both the photonic band gap and the pass band. Figure 10b shows the THG spectrum measured in the wave-vector domain. The TH intensity reveals a strong enhancement at $\theta \approx 55^\circ$ that is close to the MC mode and a resonance in SHG located at $\theta \approx 58^\circ$. The THG peak is approximately two times broader than the MC mode drop in linear reflection. This is apparently associated with the *Q*-factor values for the *p*-polarized fundamental radia-

tion being smaller than those for the *s*-polarized one. The TH intensity increases also at $\theta < 30^\circ$. This THG growth is even stronger than the enhancement in the MC mode and corresponds to the short-wavelength PBG edge.

The primary mechanism of the SHG and THG enhancement in the MC mode is the fundamental light localization inside the MC spacer and the surrounding layers of the Bragg reflectors. The partial contributions to the total harmonic field of the MC spacer and the surrounding layers of the Bragg reflectors are obtained within the nonlinear transfer-matrix formalism [31]. It is shown that the phase shift between dominating harmonic-wave contributions does not exceed $\pi/2$ providing their constructive interference. In a certain sense, this interference is equivalent to phase matching since the optical thickness of the MC spacer is effectively *Q* times extended in the MC mode.

The harmonic peaks at the PBG edge and at the minima in the reflection spectrum are treated as resonances in photonic crystals due to the small role of the MC spacer in the formation of the PBG edge. The fundamental field penetrates efficiently into photonic crystals of MC at these spectral positions, and the SHG and THG enhancement stems from constructive interference of the partial harmonics contributions of layers of the Bragg reflectors, which accomplishes effective phase matching. Additional enhancement of the amplitudes of the partial SH (TH) fields is provided due to the fundamental field localization in the finite-size photonic crystals [6]. Absorption in porous silicon at the SH (TH) wavelength varies both the amplitude and the phase of the partial harmonic wave fields, lessening the amplitude of the SHG (THG) peaks.

5. CONCLUSIONS

We have surveyed the recent studies of enhanced second- and third-harmonic generation in three types of one-dimensional photonic band-gap structures formed from mesoporous silicon. The samples fabricated by the electrochemical technique are photonic crystals consisting of quarter-wavelength-thick layers, photonic-crystal microcavities with a half-wavelength-thick microcavity spacer, and a series of coupled microcavities with two identical cavity spacers and coupling controllable by intermediate Bragg reflector transmittance. Second-harmonic spectra of the structures are studied in the fundamental wavelength range from 730 to 1050 nm. An increase in second-harmonic intensity is observed for the fundamental wavelength at the PBG edge up to 50 times in comparison with the off-resonant value outside the PBG. The matrix formalism analysis shows that the effect is caused by effective compensation of the phase mismatch at the PBG edge and by enhancement of the fundamental field inside the structure. The ratio of the resonant SH intensity in the MC mode to the off-resonant one reaches 130 times resulting from strong localization of the field at the microcav-

ity spacer. A monotonic dependence of the MC mode splitting on the transmittance of the intermediate Bragg reflector is observed in the SH angular spectra of coupled microcavities. Constructive interference of the outgoing SH fields from the various layers of CMC results in redistribution of the amplitudes of SHG resonances and their shift from the angular positions corresponding to the maximal localization of the fundamental field. Finally, the experimental observation of third-harmonic generation in PBG materials is presented. The resonant enhancement is observed both at the PBG edge and in the MC mode. The intensity reaches 10^3 at the photonic band-gap edge and 5×10^3 in the MC mode in comparison with an off-resonant value. The presence of the critical point E'_0/E_1 of silicon at approximately 360 nm results in competition between two opposite factors, i.e., high cubic susceptibility and strong adsorption of the ultraviolet TH wave in porous silicon, reducing the amplitude of the THG peaks.

ACKNOWLEDGMENTS

The authors are pleased to acknowledge V.A. Yakovlev for donating several microcavity samples. This work was supported by the Russian Foundation for Basic Research and a Presidential Grant for Leading Russian Scientific Schools.

REFERENCES

1. Y. Shen, *The Principles of Nonlinear Optics* (Wiley, New York, 1984; Nauka, Moscow, 1989).
2. S. Zhu, Y. Zhu, Y. Qin, *et al.*, Phys. Rev. Lett. **78**, 2752 (1997).
3. *Surface Enhanced Raman Scattering*, Ed. by R. K. Chang and T. E. Furtak (Plenum, New York, 1982).
4. K. Sakoda, *Optical Properties of Photonic Crystals* (Springer, Berlin, 2001).
5. A. V. Andreev, A. V. Balakin, I. A. Ozheredov, and A. P. Shkurinov, Phys. Rev. E **63**, 016602 (2000).
6. M. Centini, C. Sibilia, and M. Scalora, Phys. Rev. E **60**, 4891 (1999).
7. L. A. Kuzik, V. Yakovlev, and G. Mattei, Appl. Phys. Lett. **75**, 1830 (1999).
8. A. Fainstein, B. Jusserand, and V. Thierry-Mieg, Phys. Rev. Lett. **75**, 3764 (1995).
9. J. A. Armstrong, N. Bloembergen, J. Ducuing, and P. S. Pershan, Phys. Rev. **127**, 1918 (1962).
10. J. P. van der Ziel and M. Ilegems, Appl. Phys. Lett. **28**, 437 (1976).
11. Y. Dumeige, P. Vidakovic, S. Sauvage, *et al.*, Appl. Phys. Lett. **78**, 3021 (2001).
12. P. K. Kashkarov, L. A. Golovan, A. B. Fedotov, *et al.*, J. Opt. Soc. Am. B **19**, 2273 (2002).
13. A. V. Balakin, V. A. Bushuev, N. I. Koroteev, *et al.*, Opt. Lett. **24**, 793 (1999).
14. T. V. Dolgova, A. I. Maidikovski, M. G. Martemyanov, *et al.*, Appl. Phys. Lett. **81**, 2725 (2002).
15. V. V. Konotop and V. Kuzmiak, J. Opt. Soc. Am. B **16**, 1370 (1999).
16. M. Scalora, M. J. Bloemer, A. S. Manka, *et al.*, Phys. Rev. A **56**, 3166 (1997).
17. O. Bisi, S. Ossicini, and L. Pavesi, Surf. Sci. Rep. **38**, 1 (2000).
18. C. Mazzoleni and L. Pavesi, Appl. Phys. Lett. **67**, 2983 (1995).
19. T. V. Dolgova, A. I. Maidikovski, M. G. Martemyanov, *et al.*, J. Opt. Soc. Am. B **19**, 2129 (2002).
20. T. V. Dolgova, A. I. Maidikovski, M. G. Martemyanov, A. A. Fedyanin, and O. A. Aktsipetrov, JETP Lett. **75**, 17 (2002).
21. L. Pavesi, G. Panzarini, and L. Andreani, Phys. Rev. B **58**, 15 794 (1998).
22. M. Ghulinyan, C. J. Oton, Z. Gaburro, *et al.*, Appl. Phys. Lett. **82**, 1550 (2003).
23. D. G. Gusev, I. V. Soboleva, M. G. Martemyanov, *et al.*, Phys. Rev. B **68**, 233303 (2003).
24. M. G. Martemyanov, T. V. Dolgova, A. A. Fedyanin, JETP **98**, 463 (2004).
25. O. A. Aktsipetrov, A. V. Melnikov, Y. N. Moiseev, *et al.*, Appl. Phys. Lett. **67**, 1191 (1995).
26. M. Falasconi, L. C. Andreani, A. M. Malvezzi, *et al.*, Surf. Sci. **481**, 105 (2001).
27. Y. E. Lozovik and A. V. Klyuchnik, in *The Dielectric Function of Condensed Systems*, Ed. by L. V. Keldysh, D. A. Kirzhnits, and A. A. Maradudin (North-Holland, Amsterdam, 1989).
28. S. Nakagawa, N. Yamada, N. Mikoshiba, and D. E. Mars, Appl. Phys. Lett. **26**, 2159 (1995).
29. N. Bloembergen, R. Chang, S. Jha, and C. Lee, Phys. Rev. **174**, 813 (1968).
30. A. G. Cullis, L. T. Canham, and P. D. J. Calcott, J. Appl. Phys. **82**, 909 (1997).
31. D. S. Bethune, J. Opt. Soc. Am. B **6**, 910 (1989).